JMEPEG (2012) 21:2106–2116
DOI: 10.1007/s11665-011-0119-6

1059-9495/$19.00

Acoustic Emission Methodology to Evaluate the Fracture Toughness in Heat Treated AISI D2 Tool Steel

Sajad Mostafavi, Mohamad Fotouhi, Abed Motasemi, Mehdi Ahmadi, and Cevat Teymuri Sindi

(Submitted April 4, 2011; in revised form August 21, 2011)

In this article, fracture toughness behavior of tool steel was investigated using Acoustic Emission (AE) monitoring. Fracture toughness (K_{IC}) values of a specific tool steel was determined by applying various approaches based on conventional AE parameters, such as Acoustic Emission Cumulative Count (AECC), Acoustic Emission Energy Rate (AEER), and the combination of mechanical characteristics and AE information called sentry function. The critical fracture toughness values during crack propagation were achieved by means of relationship between the integral of the sentry function and cumulative fracture toughness (KICUM). Specimens were selected from AISI D2 cold-work tool steel and were heat treated at four different tempering conditions (300, 450, 525, and 575 °C). The results achieved through AE approaches were then compared with a methodology proposed by compact specimen testing according to ASTM standard E399. It was concluded that AE information was an efficient method to investigate fracture characteristics.

Keywords acoustic emission, critical fracture toughness, sentry function, tool steel

1. Introduction

One of the most common types of tool steel that is used comprehensively for applications when high strength, hardness, and wear resistance are required is AISI D2 cold-work tool steel. AISI D2 is a high-chromium, high-carbon tool steel alloyed with vanadium and molybdenum characterized by high compressive strength, high wear resistance, good through-hardening properties, good resistance to tempering-back, and high stability in hardening. Additionally, this kind of steel is utilized for tools requiring very high wear resistance but because of the high alloying content, it is combined with moderate toughness (shock resistance). However, the fracture toughness and microstructure depend on tempering parameters, and improving these parameters can lead to considerable effect on wear resistance, strength, and fracture toughness (Ref 1-4).

AE is the result of transient elastic wave propagation caused by a quick release of energy inside the material. It can be generated during crack nucleation and growth, twin formation, deformation, etc.

The capacity of material to resist deformation or carry loads, in the presence of a crack, is defined as the fracture toughness. Many standards are available which utilize load-displacement plot to evaluate the fracture resistance of the materials.

Sajad Mostafavi, Mohamad Fotouhi, Abed Motasemi, Mehdi Ahmadi, and **Cevat Teymuri Sindi**, Non-destructive Testing Laboratory, Department of Mechanical Engineering, Amirkabir University of Technology, 424 Hafez Ave, 15914 Tehran, Iran. Contact e-mails: ahmadin@aut.ac.ir and timuri.j@gmail.com.

AE technique has proven to be an outstanding diagnostic device for real-time monitoring of the fracture process. Extensive work has been carried out based on this technique to investigate fracture mechanisms (Ref 5-11). The approaches that were applied in the present study were based on AE methods including Acoustic Emission Cumulative Count (AECC), Acoustic Emission Energy Rate (AEER), and Sentry function, which utilizes the combination of mechanical behavior and AE information. AECC and AEER are related to acoustic emission counts and energy distribution during compact tension test. Sentry function is a method that considers the continuous balancing between the released acoustic energy due to damage and the stored strain energy (Ref 12-15). As damage intensity increases due to internal failure, the cumulated AE energy increases and the strain energy storing decreases simultaneously. There are several investigations about AE monitoring of conventional fracture toughness tests (Ref 16-19). Some of these studies have used Acoustic Emission Counts Rate (AECR) characteristic to obtain the Critical fracture toughness value, but considerable differences between ASTM standard method and AE technique have been reported.

Sentry function has been successfully applied to study damage progression and fracture energy release rate (G_I) of composite laminates. This technique was used to estimate the residual strength of a composite materials subjected to indentation processes and lateral impact (Ref 12, 14, 15). However, almost no studies have applied sentry function to investigate steels.

In this study, AE techniques and ASTM standard E399 have been utilized to study fracture mechanisms and plain strain fracture toughness of AISI D2 cold-work tool steel in various tempering temperatures. The AE analyses and procedure of ASTM E399 in terms of fracture toughness have been used to calculate the critical load value (P_Q). The critical load values related to AE techniques were calculated using four approaches:

(a) AECC
(b) AEER

(c) Integral of the sentry function (Int(f)) which is a parameter used to study material damage (Ref 14, 15). The Int(f) is the integral of the sentry function over the displacement area where AE signals have been identified:

$$\mathrm{Int}(f) = \int_{\Omega\mathrm{AE}} f(x)dx \qquad \text{(Eq 1)}$$

where ΩAE is the interval in the load-displacement diagram at which AE signals appeared. A considerable bi-linear relationship between the integral of the sentry function over the displacement domain and the cumulative fracture toughness (KICUM) can be observed. The recorded data during the test at different loads were used to calculate the KI values and KICUM is sum of these values. In this bilinear relationship, a transition point appeared that can be the basis of critical load value calculation.

(d) Guidelines recommended by ASTM E399 standard test.

Finally, the critical load values calculated by these approaches were used to determine K_{IC} values offered by ASTM E399 standard test method. Subsequently, results obtained by these approaches were compared with each other. It was concluded that a very good agreement between the results from these approaches to the ones obtained by the ASTM E399 exist.

2. Experimental Procedure

2.1 Materials Specification

In this investigation, the specimens were selected from AISI D2 Cold-Work tool steel, in the size of 50 × 50 mm and then heat-treated in the following procedure: Annealing (heating to 900 °C, keeping for 2 h, cooling slowly to 775 °C, keeping for 6 h and cooling very slowly by air); Austenitizing (heating to 1010 °C, keeping for 15 min and cooling very slowly by air); Double Tempering (keeping the selected specimens at 300, 450, 525, and 575 °C each time for 1 h and cooling by air). It should be considered that the second time, tempering temperature was 50 °C lower than the first time.

Chemical composition of the selected AISI D2 tool steel was analyzed and the results are available in Table 1.

2.2 Fracture Toughness Test

After preparing the specimens, compact tension tests were prepared to obtain fracture toughness values. Specimens were selected in size of 36 × 34 mm and 8 mm as thickness. Figure 1 shows schematics of AE setup and the compact tension test of the specimens.

According to the ASTM standard E399, if the following relation holds true, plain-strain condition can be achieved:

$$b \geq 2.5(K_Q/\sigma_{ys})^2 b \qquad \text{(Eq 2)}$$

In this relation, K_Q refers to the conditional fracture toughness, σ_{ys} refers to the material's yield strength and b refers to the specimen thickness.

Based on the ASTM standard E399 (Ref 20), crack starter was inserted in all specimens (see Fig. 1); additionally the a/w value should be equal to 0.5 where a refers to crack length and w refers to width of the specimen. All tests were carried out on a servo-electric Instron machine, at the load rate of 0.2 mm/min and at a temperature of about 25 °C. For calculating fracture toughness values, Load-Crack Mouth Opening Displacement (CMOD) data of all specimens were recorded using the actuator.

2.3 AE Equipment

AE signals were recorded using a Physical Acoustics Corporation (PAC) PCI-2 system with AE software AEWin. For monitoring AE events, three broadband, resonant-type, piezoelectric sensors with 40 dB pre-amplification and a threshold level of 20 dB for the filter were used in AE tests. The first sensor was coupled to the specimen and two others were coupled to machine jaws by means of petroleum jelly for detecting machine noises. The surfaces of sensors were covered with grease to provide good acoustic coupling between the specimen and sensors. Attached position of the AE sensors on the samples is shown in Fig. 1.

2.4 Microstructure and Fractography Investigation

Optical microscopy was utilized for investigating the microstructure of the fractured specimens which were heat-treated in various conditions. Specimens were polished mechanically, then etched with 4% Nital reagent. Subsequently, fractography examination using scanning electron microscopy (SEM) was carried out near the central plane of the fractured surface of each tested specimen to identify the fracture mechanism of the specimens.

3. Sentry Function

Sentry function expresses the combination of acoustic emission information and mechanical characteristics which is defined as the logarithm of the ratio between mechanical and acoustic energies (Eq 3) (Ref 13):

$$f(x) = \mathrm{Ln}\left[\frac{E_s(x)}{E_a(x)}\right] \qquad \text{(Eq 3)}$$

where $E_s(x)$ refers to the strain energy, $E_a(x)$ refers to the AE events energy, and x refers to the displacement. As described in previous studies (Ref 12-15), the function f is defined over the displacement domain in which acoustic energy is released.

Table 1 Chemical composition of the studied AISI D2 tool steel (wt.%)

C	Si	Mn	P	S	Cr	Ni	Mo	Al	Co
1.53	0.322	0.238	0.019	0.007	11.80	0.152	0.783	0.032	0.022
Cu	Nb	Ti	V	W	Pb	Sn	Ca	Ta	Fe
0.14	0.005	0.006	0.798	0.004	0.001	0.048	0.001	0.004	Base

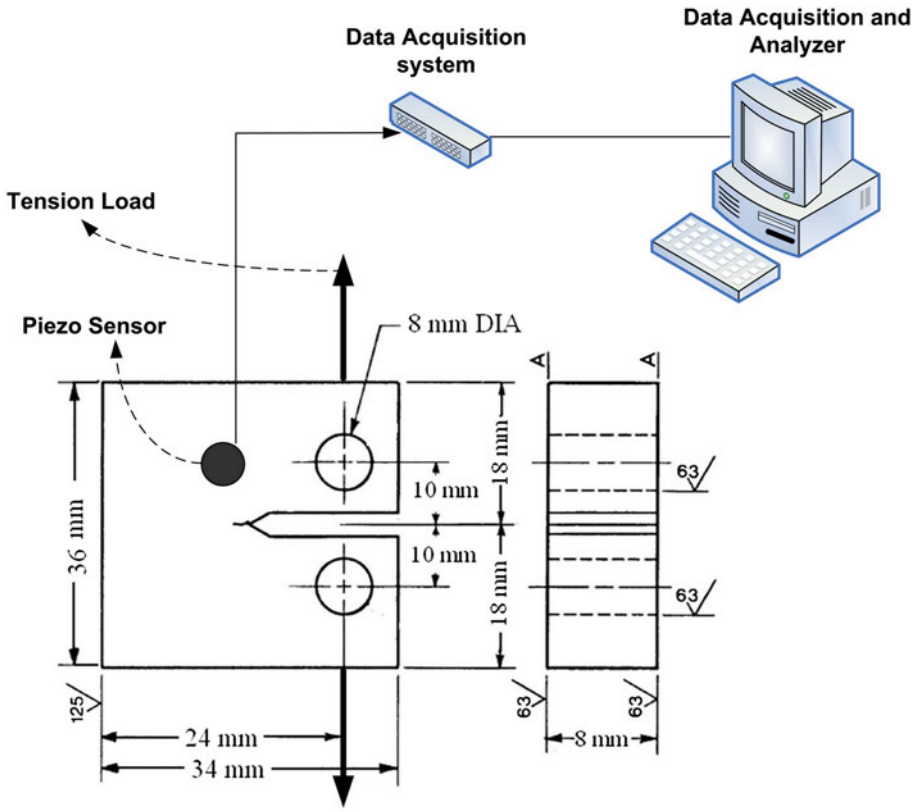

Fig. 1 Schematics of the $C(T)$ tension test specimens and AE setup

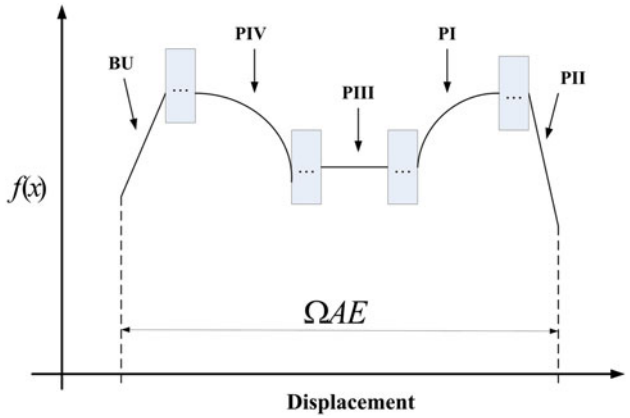

Fig. 2 Different behaviors of sentry function

The sentry function f represents five different behaviors: (1) Increasing phase, defined by PI(x), related to strain energy storing. (2) Sudden drops phase, defined by PII(x), related to an immediate release of stored energy due to internal material failure. (3) Constant phase, defined by PIII(x), related to the progressive strain energy storing due to material damage progression. (4) Bottom-Up phase, defined by (BU), related to the instantaneous energy storing capability in the material induced by strengthening event. Such an event can be caused by self-healing effects, hardening effects or, etc. (5) Decreasing phase, defined by PIV(x), related to the fact that the material strain energy storing ability is lower than the AE activity (Ref 13) (Fig. 2).

4. Results and Discussion

4.1 Calculation of K_{IC} Value Using ASTM Standard E399

Based on ASTM standard E399, Plain strain fracture toughness tests were applied on all specimens (Ref 17). The procedure for calculating the critical load (P_Q) and load-CMOD plots of specimen A2, have been shown in Fig. 3.

As it has been presented in Fig. 3, after plotting tangent line through the initial linear part of the origin of the recorded load-CMOD plot (Fig. 3a), the secant line with the slope of 0.95 the line plotted in Fig. 3(a) have been drown (Fig. 3b). The critical load is considered as the maximum intersection point of the load and tangent line in Fig. 3(b).

Subsequently, the conditional value of fracture toughness according to the standard E399 is calculated using Eq 4:

$$K_Q = \left(\frac{P_Q}{BW^{0.5}}\right) \times f\left(\frac{a}{W}\right) \quad \text{(Eq 4)}$$

where $f(a/W)$ is defined by Eq 5:

$$f\left(\frac{a}{W}\right) = \frac{\left(2+\frac{a}{W}\right) \times \left(0.886 + 4.64\frac{a}{W} - 13.32\frac{a^2}{W^2} + 14.72\frac{a^3}{W^3} - 5.6\frac{a^4}{W^4}\right)}{\left(1-\frac{a}{W}\right)^{1.5}} \quad \text{(Eq 5)}$$

Critical load, yield strength, conditional fracture toughness values, and P_{max}/P_Q ratio are listed in Table 2.

Tension tests were carried out according to the procedure of ASTM standard E8-01 (Ref 21) to determine (σ_{ys}) values at different tempering conditions. By estimating K_Q and σ_{ys} values of the selected steel in various tempering temperatures,

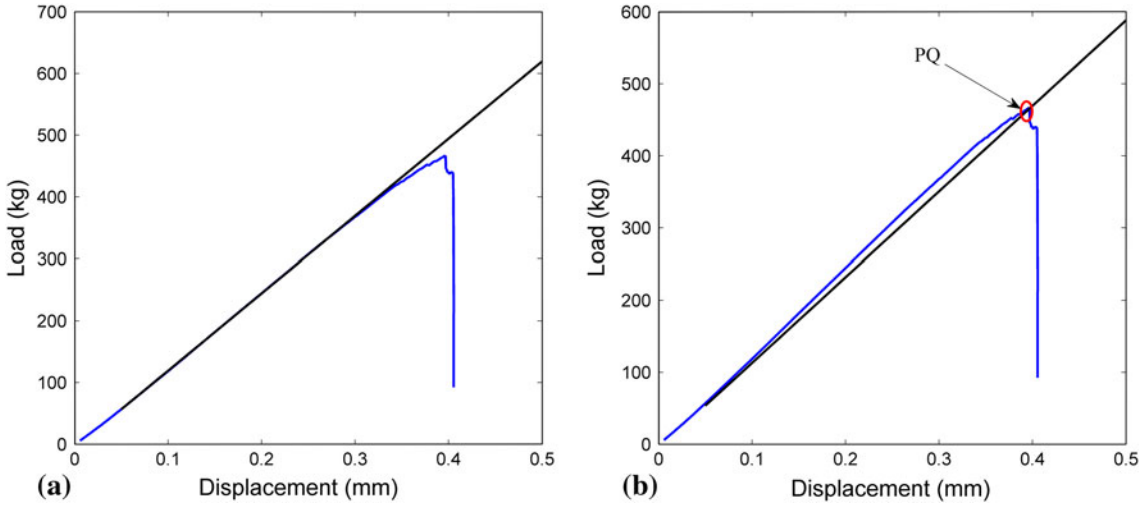

Fig. 3 Load-CMOD plot of specimen A2: (a) tangent line and (b) the secant line with slope of 0.95 of the tangent line

Table 2 The results of fracture toughness measurement of the D2 steel according to ASTM standard E 399

Sample no.	σ_{ys}, MPa	P_Q, kN	K_Q, MPa$\sqrt{m}$	$\frac{P_{max}}{P_Q}$	$2.5\left(\frac{K_Q}{\sigma_{ys}}\right)^2$, mm	K_{IC} Each one	K_{IC} Average
D1	1760	4.89	35.52	< 1.15	1.02	35.52	35.28
D2		5.05	35.76	< 1.15	1.03	35.76	
D3		4.92	34.56	< 1.15	0.96	34.56	

the minimum thickness required for valid K_{IC} measurement which is derived from equations (2, 3), is shown in Table 2.

4.2 Fractography

As shown in Fig. 4, all specimen surfaces contain a combination of ductile fibrous fracture and brittle cleavage on the primary carbides. The highest percentage of brittle cleavage fracture occurs in the specimen without tempering (Fig. 4a).

Increasing tempering temperature leads to an increase of dimples on surfaces (ductile fracture) together with increasing fracture toughness values (Fig. 4b). As shown in (Fig. 4c) due to presence of secondary hardening event at 525 °C, there is cleavage type of fracture on the secondary carbides. This structure decrease the toughness value (Fig. 4c) and is the main cause of irregular behavior of the investigated steel. By increasing tempering temperature, ductile fracture (dimple formations on fracture surfaces) increases (Fig. 4d).

4.3 Fracture Toughness Values Determination by AE Technique

As it can be recognized from AE count versus time plot (see Fig. 5), by increasing loading rate various mechanisms influence the fracture process. Analysis of AE plots of fracture toughness tests of AISI D2 tool steel indicated that three specific regions appeared. These regions were:

Region 1: Weak AE peaks occurred because the specimen was still in elastic state.

Region 2: Relatively high energy signals were generated in the second region, which is probably related to the microcracks initiation and propagation due to low plastic deformation and high strength at the crack tip of the specimens.

Region 3: AE energies reach their maximum value in this region because of the quick and unstable crack propagation.

These three regions are shown on AE counts-time plot of the specimen A2 in Fig. 5.

Determination of critical load value by means of AE technique was utilized for calculating fracture toughness. In previous investigations (Ref 22-24) almost all studies have used the point related to the first jump instead of the critical load in AE cumulative counts plot. Albeit considering first jump has some advantages in determining fracture toughness values, in some cases, some considerable differences occurred between fracture toughness values calculated using first jump method in comparison with the standard ASTM E399 results. Figure 6 demonstrates the points of critical load according to the first jump for specimen C2.

According to our previous study in this field (Ref 11), AEER technique offers better results compared with previous studies. In this approach, the critical load ($P_{Q,AEER}$) was considered as the load matching to the point having the maximum value of AE energies rate versus time, before sudden drop of load. Figure 7 shows this method to investigate fracture toughness value of the specimen D2.

To create a more accurate method to calculate the critical load from AE events, a novel approach which is the combination of mechanical behavior and AE information called sentry function was applied. Also this method was used to study different fracture mechanisms of different specimens.

4.4 Sentry Function

4.4.1 Sentry Function Trends. The sentry function is the logarithm of the ratio between the strain energy and the cumulative acoustic energy as in Eq 1. Sentry function trends obtained in the case of different specimens tempered at 0, 300, 450, 525, and 575 °C are shown in Figs. 8, 9, 10, 11, and 12 respectively.

As it can be seen the different samples have special behaviors from acoustic point of view. It can be observed that during tensile test, there are some strain energy storing stages, BU and PI, which display ability to store strain energy.

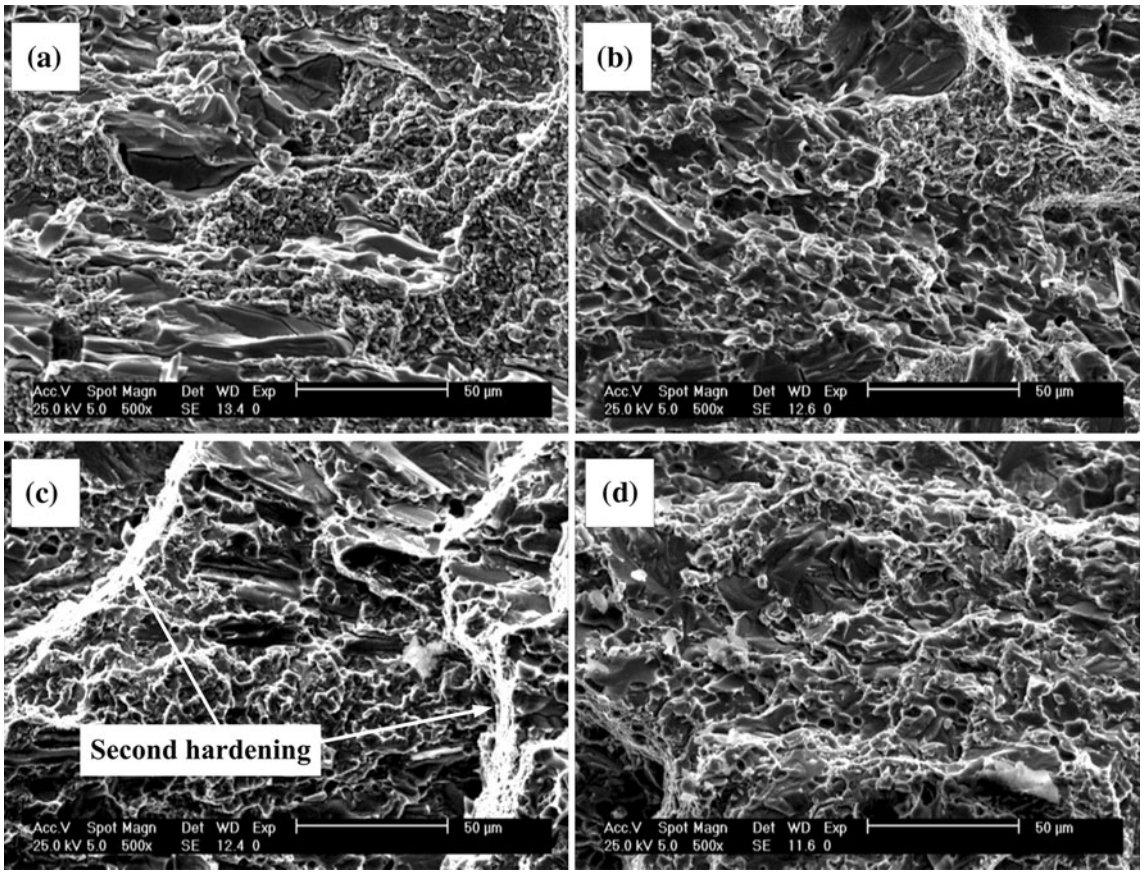

Fig. 4 SEM fractograph of: (a) A1 showing the highest fraction of brittle cleavage fracture, (b) C3 showing increase of dimples on surfaces, (c) D1 showing cleavage fracture on the secondary carbides and (d) E2 showing predominantly ductile failure

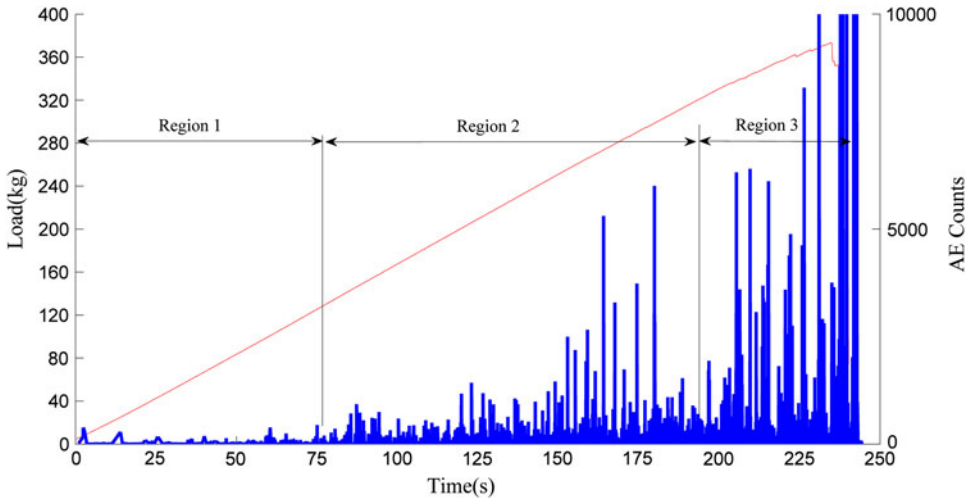

Fig. 5 Different regions on AE counts plot determine fracture mechanisms

An increase in the magnitude of the function displays strain storing ability. It is observed that specimen A retains its strain storing ability up to the displacement of 0.128 mm. This means that from the beginning of the load until 0.128 mm microcracks which did not have dominant effect in the strength of material propagated and no considerable AE events during first stage of loading were recorded and this phenomenon leads to the dramatic increase of the sentry function. This stage for specimens B, C, D, and E is extended up to 0.08, 0.43, 0.39, and 0.2 mm, respectively. As it can be seen, almost in each sample there is one continuous increasing region, except the specimen tempered at 525 °C. There is some irregularity about the trend of sentry function in specimens tempered at 525 °C. This different behavior can be related to the presence of significant secondary hardening phase which causes two separate increasing regions.

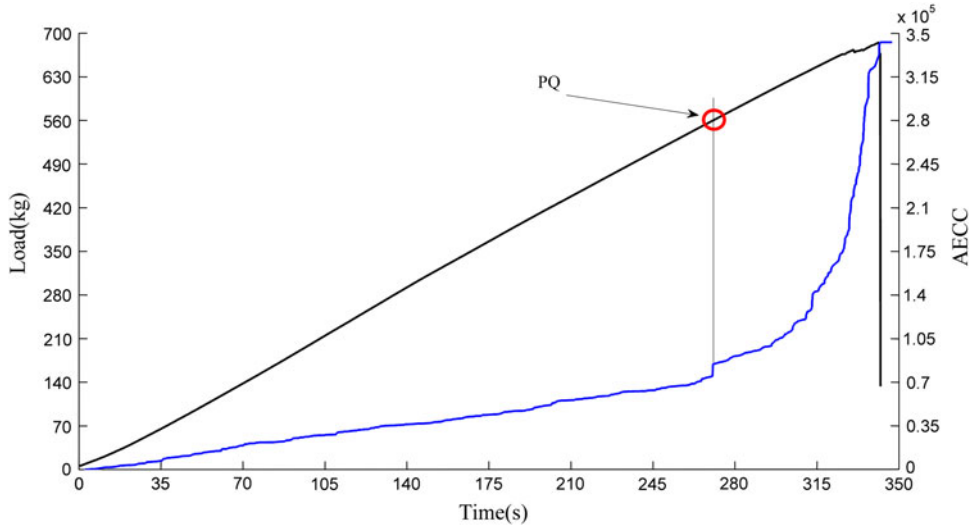

Fig. 6 Estimation of critical load (P_Q) according to conventional AE technique for specimen C2

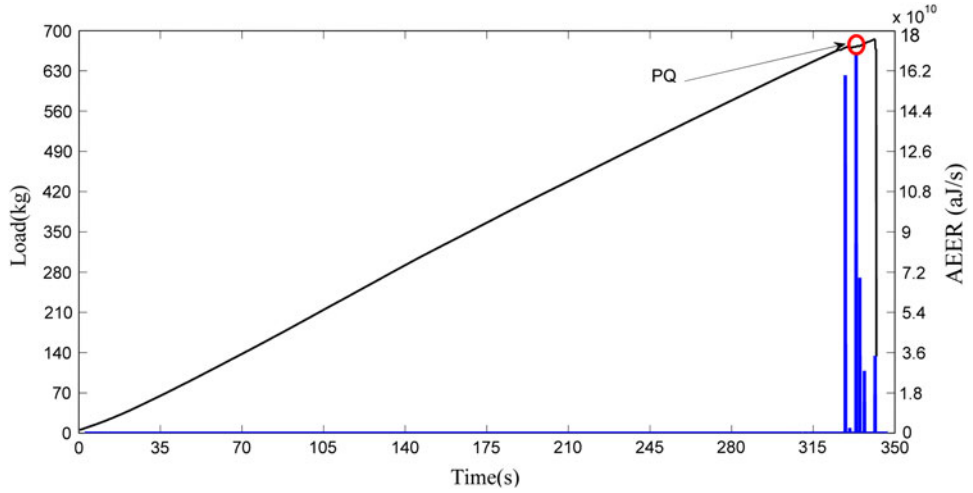

Fig. 7 Determination of critical load (P_Q) for specimen D2 using AEER technique

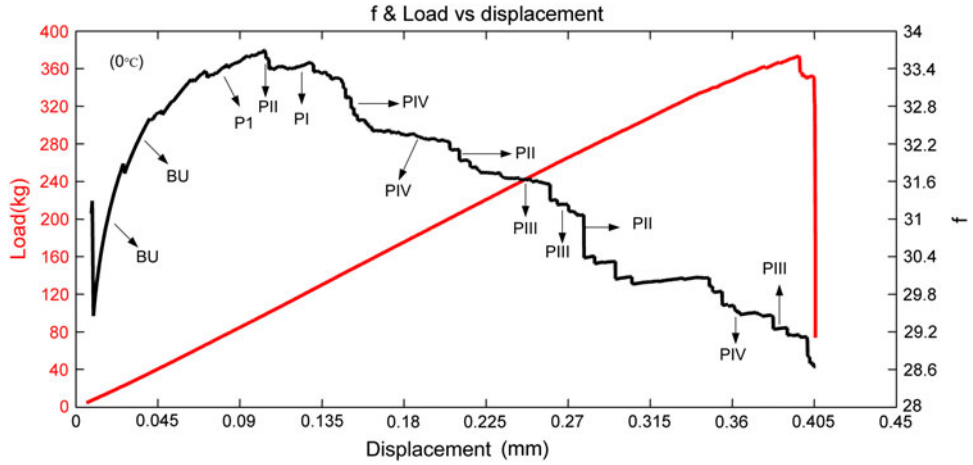

Fig. 8 Sentry function trends obtained in the case of specimen tempered at 0 °C

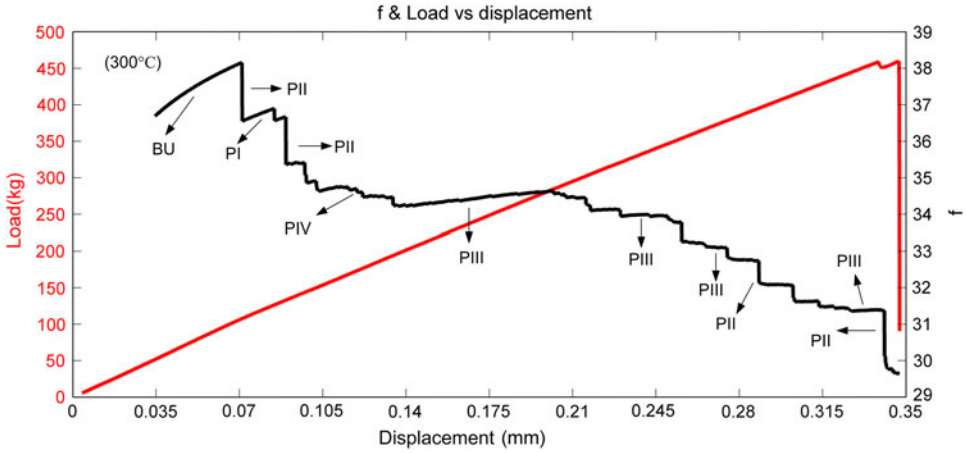

Fig. 9 Sentry function trends obtained in the case of specimen tempered at 300 °C

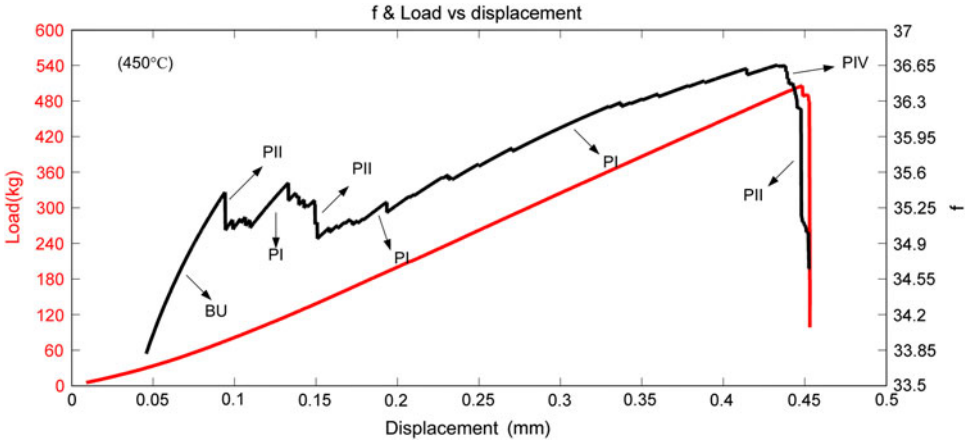

Fig. 10 Sentry function trends obtained in the case of specimen tempered at 450 °C

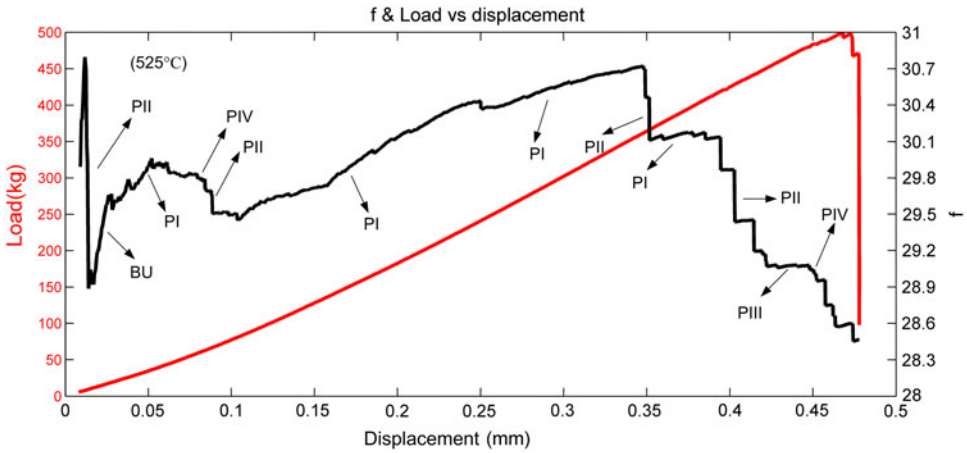

Fig. 11 Sentry function trends obtained in the case of specimen tempered at 525 °C

After the strain energy storing phase there are PIV trends, which indicate that the structure is damaged and has lost its ability to store more energy, this stage specifies that the released AE energy tends to overcome the strain energy storing capability of the material. In specimens A, B, and E this stage is extended from 0.128, 0.08, and 0.2 mm until the maximum load, respectively. Also, the slope of sentry function trend in specimen A is greater than specimen B and slope of B is greater than E. This means that for brittle materials the slope of sentry function is higher than for ductile materials. This event is because of unstable crack extension in brittle materials. Energy release rate in brittle materials is higher than ductile materials.

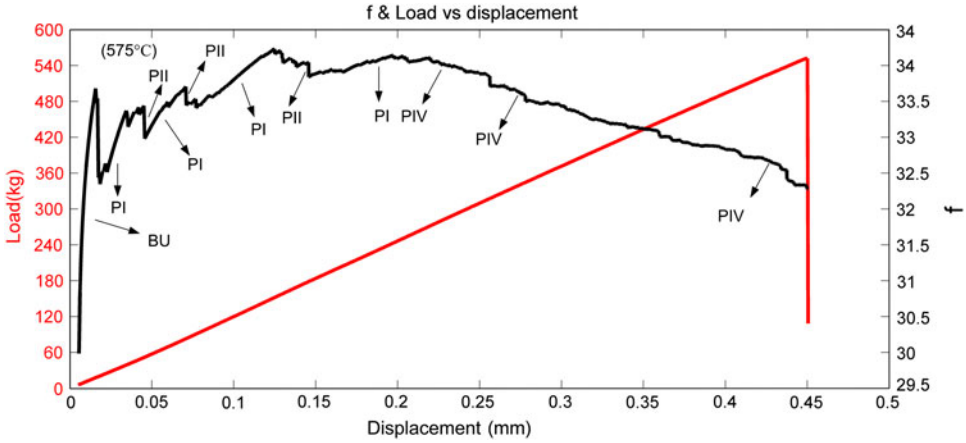

Fig. 12 Sentry function trends obtained in the case of specimen tempered at 575 °C

For specimens C and D, the trends are completely different and this stage only appears near the maximum load. Also, the slope of sentry function trend decreases significantly. This diverse behavior can be associated with the presence of secondary hardening which causes sudden release of AE energy.

In addition, there are some PII trends from beginning of loading until the maximum load. Type II function, represented by a sudden drop, indicates a failure in the material. This is because when a major crack propagates, large amount of energy is suddenly released in the material; a portion of that energy produces high energy AE events. It is clear from the samples that after each damage event, type II function, the energy storing ability of the material declines but does not completely diminish until the slope approaches zero or becomes negative.

The type III function, represented by a constant function, indicates smooth propagation in tensile test and shows that the failure mechanism is unvarying. Ductile specimens, C and E, have negligible type III functions, A and D have several type III at the final stages while the majority of the functions in B is type III.

4.4.2 An Alarm to Avoid Fracture. Int(f) which is the integral of the sentry function diagram over the AE displacement domain is a good tool for studying material damage (Ref 12, 13). Based on previous examination, the integral of the sentry function is related to the test stage at which the crack initiated. By applying this method, the integral of the sentry function was obtained between the displacement at which the AE signals were recorded for the first time and the displacement at which the crack initiated (point having the maximum value of AE energies rate).

From Fig. 13, it can be observed that the sentry function integral values, between the first appearance of AE events and the point having the maximum value of AE energies rate, has little difference from the mean value for various temperatures. Also there is a similar behavior in variation of the K_{IC} values obtained from Table 2 and variation of the Int(f) values obtained from Fig. 13. This similarity is due to the fact that by increasing tempering temperature there is increase in the value of this integral except at 525, so K_{IC} values and values obtained using Int(f) have proportionality. In accordance with these results, sentry function integral value can be used as an alarm for the initiation of crack. Practically, this method could be suitably used for the detection of the crack initiation in a real structure.

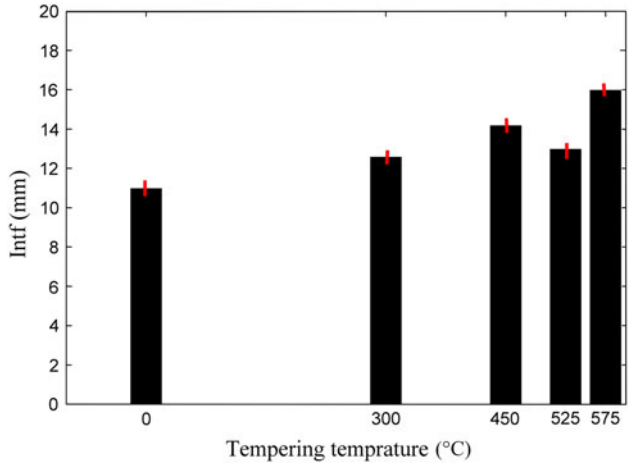

Fig. 13 Mean values and standard deviation of the integral of the sentry function between the beginning of the AE and the first visible crack propagation

4.4.3 Calculation of Fracture Toughness (K_{IC}) Value. In Fig. 14 the relationship between the fracture toughness and the integral of the sentry function is shown. This plot is the basis for determination of the K_{IC} value.

In a previous study (Ref 12), this trend which is based on a bi-linear relationship (using a linear fitting of the data) between the KICUM and Int(f) was used successfully to determine the delamination fracture toughness at mode I in composite laminates. Therefore utilizing the plots in Fig. 14 it is feasible to evaluate the K_{IC} values in steel.

As is shown in Fig. 14, Int(f) and KICUM, show a proportionality. Proportionality is due to the fact these two variables are correlated with the material damage. The KICUM is defined as the capacity of material to resist deformation or carry loads, in the presence of a crack, and the Int(f) is concerned with the material damage (Ref 12, 13). Considering the KICUM values of the specimens in transition points (Fig. 14), it can be seen that specimens tempered at 575 °C are the toughest ones. The slope of the fitting line before and after the transition point has some variation for all of the specimens. This variation is related to a change of the capacity of the material to resist deformation (crack initiation). According to Fig. 14 the capacity of material to resist crack propagation is

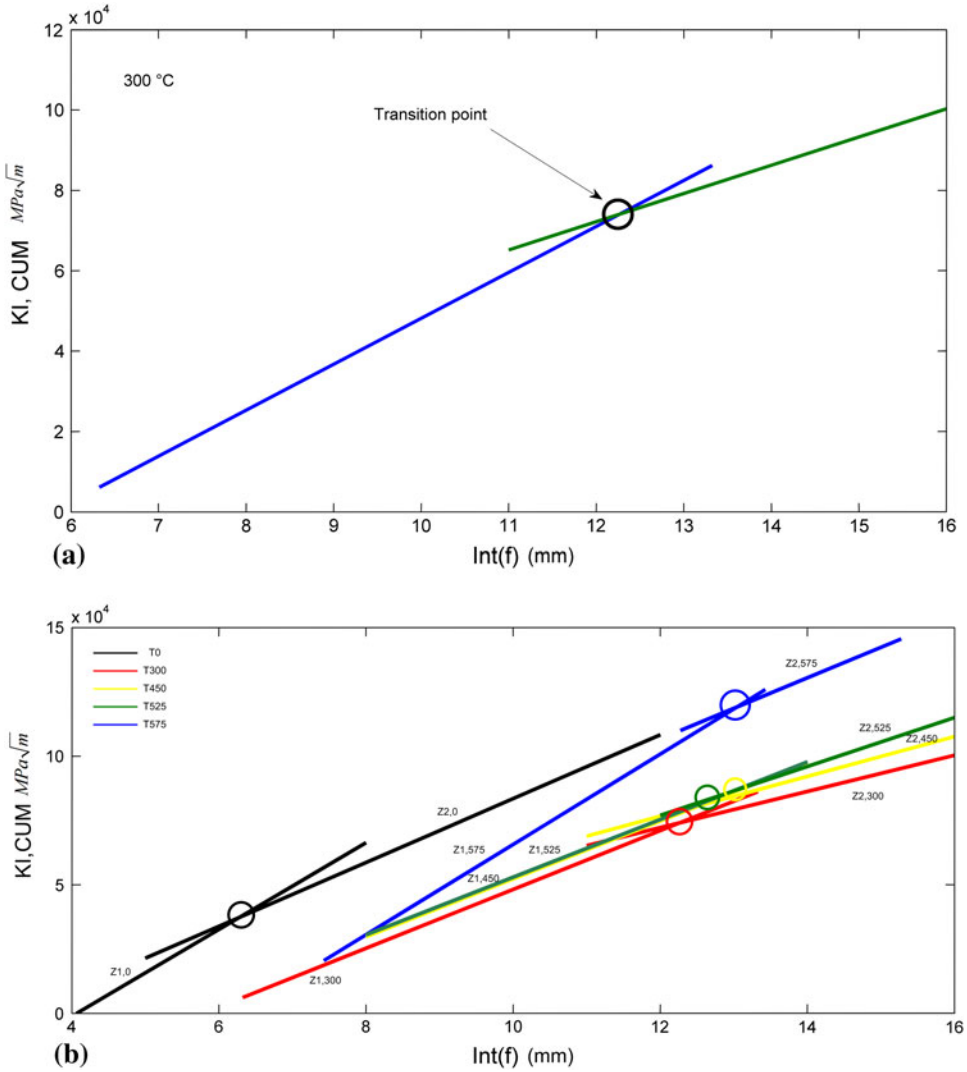

Fig. 14 (a) Plot of cumulative KI versus integration of *f* function for specimen tempered at 300; (b) plot of cumulative KI versus integration of *f* function, in this case the bilinear functions for each specimen type are visually characterized by means of the transition points highlighted by the circles

reduced after the transition points. This decrease can be observed from the fact that by small increase of KICUM, there is a considerable increase in Int(*f*).

As a result, Int(*f*)-KICUM plot can be used to calculate the K_{IC}. Results obtained using these different approaches are listed in Table 3.

Figures 15 and 16 illustrate K_{IC} values listed in Table 3. As it can be seen, AEER and sentry function techniques are more precise than AECC. In addition it can be seen that when fracture toughness values increase, the calculated fracture toughness using conventional AE methods, have more deviation. But, K_{IC} values determined by sentry function and AEER methods are independent of fracture toughness values and have excellent adjustment with ASTM E399. Furthermore, like previous studies (Ref 11), all K_{IC} values determined using AE based methods have lower value than ASTM E399 method. As stated above, in AECC technique the critical load is equal to the load related to the onset of the initial crack propagation. The critical load, $P_{Q,A}$, in AEER technique is the load obtained from the point having the maximum value of AE energies rate versus time. In the sentry function method, K_{IC} is calculated using the knee point happening in the KI cumulative versus Int(*f*) diagram. The knee point in this diagram is related to the K_{IC} that can be found from the Load-Time plot. With regard to the critical load, the K_{IC} value of the critical fracture toughness is calculated. In addition, it is interesting to note that the standard deviation associated with the results determined by the new techniques (AEER and the sentry function) are smaller compared with the results obtained using ASTM E399 method. As a result, it can be concluded that AEER and the sentry function are other alternative methods to determine K_{IC} values

Table 3 Results obtained using different approaches

Method	Fracture toughness, MPa$\sqrt{m}$				
T. T. (°C)	0	300	450	525	575
ASTM E399	23.77	29.76	35.8	35.28	46.04
AEER	23.29	29.2	35.47	34.16	46
Sentry function	23.25	29.04	35.5	34.13	45.07
AECC	23.01	27.3	31.94	33.52	38.79

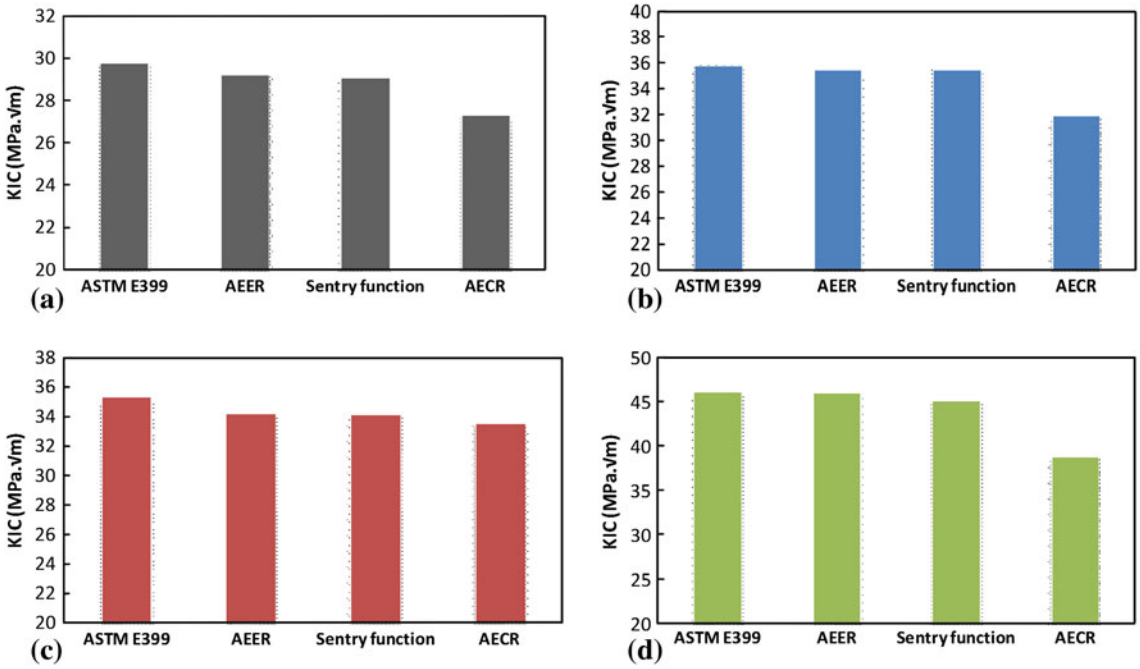

Fig. 15 Comparison between the results from the different methods for K_{IC} calculation of specimens tempered at: (a) 300 °C, (b) 450 °C, (c) 525 °C, and (d) 575 °C

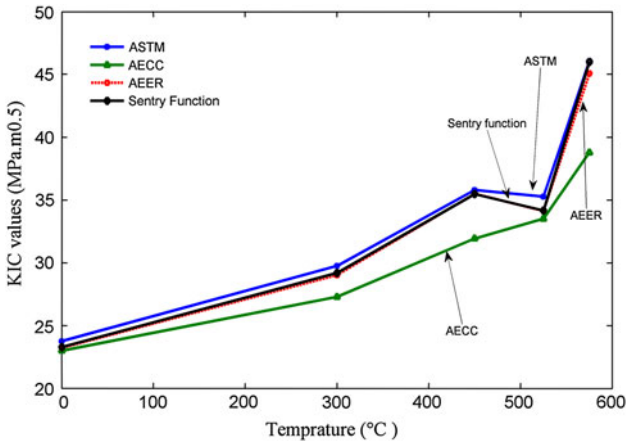

Fig. 16 Comparison of (K_{IC}) values determined according to standard ASTM E 399, AECR, AEER, and Sentry Function methods

from AE data. As results revealed, the specimens without tempering condition have lowest K_{IC} values. Because of the transformation of tempered martensite, enhancing the tempering temperature leads to the increase of plain strain fracture toughness values. At 525 °C, there is little decrease in fracture toughness irregularly. Transformation of retained austenite during tempering at the higher temperature due to secondary hardening has been the reason of this irregular decrease in fracture toughness.

5. Conclusions

The results showed that by increasing tempering temperature, transformation of tempered martensite occurs which leads to increase of K_{IC} values of AISI D2 tool steel. But at 525 °C, there is a slight decrease in fracture toughness values. This different behavior is because of secondary hardening phenomenon in this type of tool steel.

For evaluation of K_{IC} values sentry function and AEER techniques were used to obtain more accurate results than conventional AE methods. Also, the K_{IC} values obtained by the proposed methods have a lower standard deviation from the mean value in comparison with the results obtained by other techniques. In addition, sentry function is a better technique than AECC and AEER to study the different events in tensile testing. Sentry function is a new function which combines strain energy, mechanical information, the acoustical information, and the acoustic emission event energy. This technique is used to study the crack propagation of the considered specimens, and especially it was used to identify damage development for each specimen and to recognize different microstructural events like secondary hardening and microcracks in specimens with different tempering temperature. More than this, the sentry function was also used to obtain an alarm for the identification of the test stage at which the initiation of crack occurs. SEM observation shows that the fracture mechanism of tempered steel is a combination of brittle cleavage and ductile fibrous. SEM observation at 525 °C indicates secondary hardening phenomena which is the main reason for irregular trend in K_{IC} values and sentry function behavior. It was concluded that the proposed methods are robust devices to study microstructural events and to calculate K_{IC} values.

References

1. L. Bourithis, G.D. Papadimitriou, and J. Sideris, Comparison of Wear Properties of Tool Steels AISI, D2 and O1 with the Same Hardness, *J. Tribol. Int.*, 2006, **39**, p 479–489

2. D. Dasa, A.K. Duttab, and K.K. Rayc, Influence of Varied Cryotreatment on the Wear Behavior of AISI, D2 Steel, *J. Wear*, 2009, **266**, p 297–309
3. X. Ma, R. Liu, and D.Y. Li, Abrasive Wear Behaviour of D2 Tool Steel with Respect to Load and Sliding Speed Under Dry Sand/Rubber Wheel Abrasion Condition, *J. Wear*, 2000, **241**, p 79–85
4. http://www.bucorp.com/files/aisi_d2.pdf
5. H. Chang, E. Han, J.Q. Wang, and W. Ke, Acoustic Emission Study of Corrosion Fatigue Crack Propagation Mechanism for LY12CZ and 7075-T6 Aluminum Alloys, *J. Mater. Sci.*, 2005, **40**, p 5669–5674
6. C.K. Mukhopadhyay, K.V. Kasiviswanathan, T. Jayakumar, and B. Raj, Acoustic Emission During Tensile Deformation of Annealed and Cold-Worked AISI Type 304 Austenitic Stainless Steel, *J. Mater. Sci.*, 1993, **28**, p 145–154
7. Y. Blanchettea, J.I. Dicksona, and M.N. Bassim, Detection of General Yielding in a516 Steel by Acoustic Emission, *J. Eng. Fract. Mech.*, 1983, **17**, p 227–234
8. M.N. Bassim, Detection of Fatigue Crack Propagation with Acoustic Emission, *J. NDT & E Int.*, 1992, **25**, p 287–289
9. M.N. Bassima, S.S. Lawrence, and C.D. Liu, Detection of the Onset of Fatigue Crack Growth in Rail Steels Using Acoustic Emission, *J. Eng. Fract. Mech.*, 1994, **47**, p 207–214
10. V.V. Korchevskii, Measurement of the Parameters of the Acoustic Emission When Metals are Stretched Acoustic Measurements, *J. Meas. Tech.*, 2006, **49**, p 517–523
11. C.T. Sindi, M.A. Najafabadi, and S.A. Ebrahimian, Fracture Toughness Determination of Heat Treated AISI, D2 Tool Steel Using AE Technique, *J. ISIJ Int*, 2011, **51**, p 305–312
12. A. Refahi Oskouei, A. Zucchelli, M. Ahmadi, and G. Minak, An Integrated Approach Based on Acoustic Emission and Mechanical Information to Evaluate the Delamination Fracture Toughness at Mode I in Composite Laminate, *J. Mater. Des.*, 2010. doi:10.1016/j.matdes.2010.08.048
13. G. Minak and A. Zucchelli, Damage Evaluation and Residual Strength Prediction of CFRP Laminates by Means of Acoustic Emission Technique, *Composite Materials Research Progress*, L.P. Durand, Ed., Nova Science Publishers, New York, 2008, p 165–207
14. G. Minak, P. Morelli, and A. Zucchelli, Fatigue Residual Strength of Circular Laminate Graphite-Epoxy Composite Plates Damaged by Transverse Load, *Compos. Sci. Technol.*, 2009, **69**(9), p 1358–1363
15. G. Minak, S. Abrate, D. Ghelli, R. Panciroli, and A. Zucchelli, Residual Torsional Strength after Impact of CFRP Tubes, ICCE-17, *World J. Eng.*, Honolulu (HI), 26 Luglio-1 August
16. Y. Blanchettea, J.I. Dicksona, and M.N. Bassim, The Use of Acoustic Emission to Evaluate Critical Values of K and J in 7075-T651 Aluminum Alloy, *J. Eng. Fract. Mech.*, 1984, **20**, p 359–371
17. C.S. Camerini, J.M.A. Rebello, and S.D. Soares, Relationship Between Acoustic Emission and CTOD Testing for a Structural Steel, *J. NDT & E Int.*, 1992, **25**, p 127–133
18. T. Ohira, and Y.-H. Pao, Microcrack Initiation and Acoustic Emission During Fracture Toughness Tests of A533B Steel, *J. Metall. Mater. Trans. A*, 1986, **17**, p 843–852
19. X. Long, G. Cai, and L.-E. Svensson, Investigation of Fracture and Determination of Fracture Toughness of Modified 9Cr-1Mo Steel Weld Metals Using AE Technique, *J. Mater. Sci. Eng. A*, 1999, **270**, p 260–266
20. ASTM E399, *Annual Book of ASTM Standards*, Vol 03.01, American Society for Testing and Materials, New York, 2001
21. ASTM E8-01, *Annual Book of ASTM Standards*, Vol 03.01, American Society for Testing and Materials, New York, 2001
22. D. Dilipkumar, V.S.R. Gudimetla, and W.E. Wood, Amplitude-Distribution Analysis of Acoustic Emission, a Simplified Method of Amplitude-Distribution Analysis Based on Cumulative Counts and Events is Presented and a New Model for Amplitude Distribution is Proposed, *J. Exp. Mech*., 1979, **19**, p 438–443
23. M. Arii, H. Kashiwaya, and T. Yanuki, Slow Crack Growth and Acoustic Emission Characteristics in COD Test, *J. Eng. Fract. Mech*., 1975, **7**, p 551–552
24. H. Roy, N. Parida, S. Sivaprasad, S. Tarafder, and K.K. Ray, Acoustic Emissions During Fracture Toughness Tests of Steels Exhibiting Varying Ductility, *J. Mater. Sci. Eng. A*, 2008, **486**, p 562–571